Radial Transport in a Tandem Mirror

Guy Dimonte
Lawrence Livermore National Laboratory, University of California, Livermore, California 94550, and TRW Corporation, Redondo Beach, California 90278
(Received 23 November 1987)

Experiments in the tandem mirror TMX-U reveal three significant sources of nonambipolar radial transport associated with resonant transport in the central cell and, in the end cells, with electron cyclotron heating and neutral beam heating. A simple model suggests that the electron-cyclotron-heating–induced transport is due to the asymmetric application of power. This transport mechanism is important because it applies even in axisymmetric magnetic geometries.

PACS numbers: 52.55.Jd

With improved electrostatic confinement in tandem mirrors,[1,2] radial transport has become important in the determination of global confinement. Theoretically,[3,4] quadrupole magnetic fields used for MHD stability enhance the radial losses because resonant ions, which drift azimuthally by an odd multiple of $\pi/2$ each axial bounce, experience large radial geodesic curvature drifts. In TMX-U,[5] the radial loss rate $\nu_\perp$ increases with potential ϕ as expected from resonant transport (RT). However, the measured magnitude and radial variation of $\nu_\perp$ are inconsistent with RT theory. In Gamma-10,[2] a similar but weaker radial transport is observed even though the central cell is axisymmetric. Significant radial transport also occurs in RFC-XX,[6] which is fully axisymmetric.

Because of these anomalies, I examined nonambipolar radial transport in TMX-U combining a statistical data analysis with experimental variations testing the correlation results. In addition to RT, the analysis reveals two significant sources of radial transport in the end cells associated with electron cyclotron heating (ECH) and sloshing-ion neutral-beam injection.[7] A simple model calculation is presented that reproduces experimental scaling laws and indicates that asymmetric heating (ECH) can easily drive more radial transport than RT. In support of this hypothesis, I reduced the geodesic curvature[8] in TMX-U and observed only minor changes in $\nu_\perp$.

The experimental configuration has been described elsewhere.[1,7] In the end cells, ECH is performed at both the fundamental Ω and harmonic 2Ω resonances to generate the electrostatic confining potential and thermal-barrier hot electrons, respectively. For the results presented here, a Vlasov antenna[9] was used at Ω which concentrates the power in the core. End-cell neutral beams aimed at 47° with respect to the magnetic field **B** produce energetic (10 keV) sloshing ions for self-consistent charge neutralization. The central-cell plasma has a Gaussian density profile $\exp(-r^2/r_p^2)$ with $r_p = 20$ cm measured by neutral-beam attenuation. The limiter radius is $r_l = 25$ cm.

A sample discharge is shown in Fig. 1 including (a) the on-axis plasma density in the central cell n_{cc} and east (n_{ep}) and west (n_{wp}) end cells (with the assumption of Gaussian profiles); (b) the total sloshing-beam drain

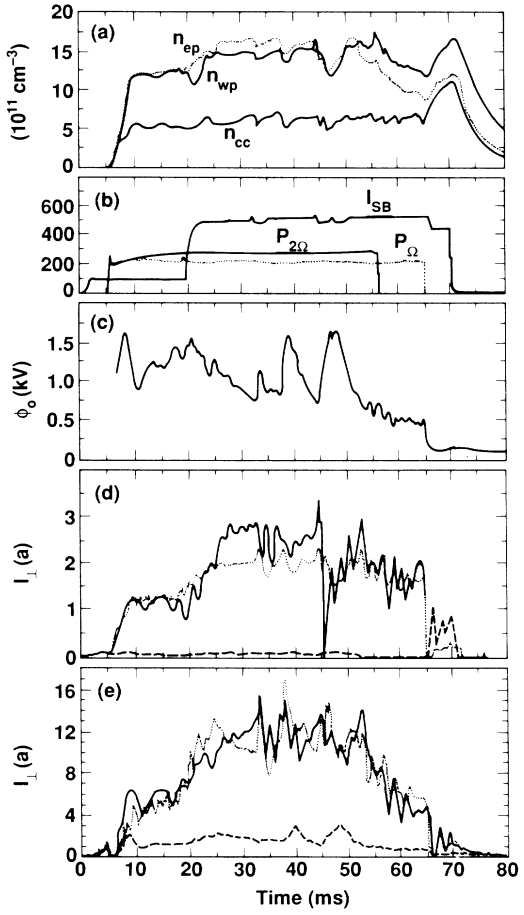

FIG. 1. Temporal variation of selected quantities for shot 8 with Vlasov antenna. Solid lines in (d) and (e) are measurements of $I_\perp$ at $r = 6.5$ and 19 cm, respectively. Dotted lines are corresponding predictions $\hat{I}_\perp$ from Eq. (1) and dashed lines are RT predictions $I_{\perp m}$ from Eq. (2).

current I_{sb} in amperes and the fundamental P_Ω and harmonic $P_{2\Omega}$ ECH power in kilowatts; (c) the peak potential ϕ_0 measured on axis with an end-loss ion spectrometer[10]; and the net outward radial ion current $I_\perp$ at (d) $r=6.5$ cm and (e) $r=19$ cm. $I_\perp$ is inferred from the integrated net electron current to segmented plasma-potential control plates[5] in the end fans. Several noteworthy features indicate that $I_\perp$ depends on P_Ω and I_{sb} in addition to ϕ_0. $I_\perp$ tracks ϕ_0 near the edge as they both decrease fourfold from 50 to 65 ms in Fig. 1(e), but not in the core since $I_\perp(6.5\text{ cm})$ decreases by only 20% over the same period. When I_{sb} increases at $t=20$ ms, $I_\perp$ doubles everywhere even though n_{cc} and ϕ_0 are relatively constant. When the fundamental ECH terminates at $t=65$ ms, $I_\perp$ decreases everywhere and the densities rise as confinement improves.

The dependence of $I_\perp$ on P_Ω, I_{sb}, ϕ_0, and densities is shown explicitly in Fig. 2. Since the Vlasov antenna concentrates the power near the axis, the correlation of $I_\perp$ with P_Ω is most clear at $r=6.5$ cm as seen in Fig. 2(a). Here, I restrict $I_{sb}<150$ for clarity since $I_\perp$ also depends on I_{sb}. To demonstrate the latter, let me define the radial confinement time $\tau_\perp=Q(r)/I_\perp$ where $Q(r)=2\pi e\int dz\, r\, dr\, n$ in the charge inside a flux tube including the end cells, n is the density, and e is the electronic charge. In Fig. 2(b), I plot $\tau_\perp$ vs ϕ_0 at $r=19$ cm for $I_{sb}<50$ A and $I_{sb}>350$ A. Indeed, $\tau_\perp$ varies as ϕ_0^{-1} but $\tau_\perp$ is smaller with higher sloshing beam current.

Figures 1 and 2 demonstrate the multidimensional nature of radial transport. In order to deal with this complexity in a quantitative manner, multiple regression analysis[11] is used to correlate $I_\perp$ with plasma and power system parameters under different operating conditions. The data base described here, called the Vlasov case, consists of 382 data sets. Each set includes heating power levels, plasma density at different axial and radial locations, axial and radial loss currents, ϕ_0, central-cell ion temperature T_i, hot-electron diamagnetism, and fueling methods. Models can be evaluated with the square of the multiple correlation coefficient R^2 but the related F statistic[11] is preferred because it compensates for the addition of new variables to the model.

In this Vlasov case, the radial current can be described by the model

$$\hat{I}_\perp = aP_\Omega^{1/3}Q^{2/3} + bn_{cc}\phi_0 + cI_{si}\phi_0 + dI_{si}, \quad (1)$$

where a, b, c, and d are constants to be determined by regression analysis at each radius. The first term represents the direct influence of ECH. The total charge is used because the density in all regions, including the central cell, is affected by P_Ω as seen in Fig. 1(a). The exponents $\frac{1}{3}$ and $\frac{2}{3}$ are movitvated by a calculation which is described later. The second term represents RT. The last two terms, which are suggested in Fig. 2(b), indicate how much of the total sloshing-ion transport is in the radial direction. The sloshing-ion loss current is $I_{si}=e\int dz\, 2\pi r\, dr\, n_{si}v_{si}$ integrated over both end cells. Their density n_{si} is measured with calibrated secondary-emission detectors. The loss rate v_{si} is inferred from the sloshing-ion rate equation with the net trapped neutral beam current. Figure 3 shows the predicted current $\hat{I}_\perp$ from Eq. (1) versus the measured current $I_\perp$ at $r=19$ cm. Typically, the points are within ± 1.6 A (residual standard deviation) of the identity line. The discrepancy may be due to the inadequacy of Eq. (1) or measurement errors.

The regression analysis is summarized in Table I. The large values of F establish the solid statistical significance of the independent variables in Eq. (1) with the confidence level exceeding 99%. The population average of each term is also shown in amperes; standard devia-

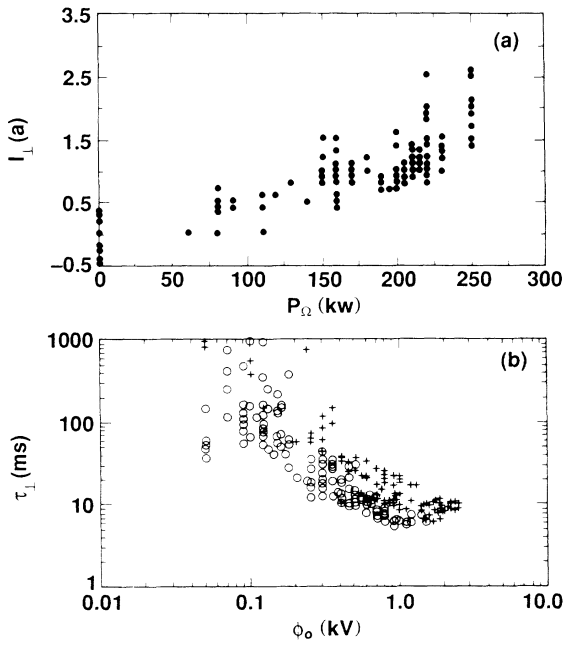

FIG. 2. (a) Variation of $I_\perp$ with P_Ω for $r=6.5$ cm. (b) $\tau_\perp$ vs ϕ_0 at $r=19$ cm with $I_{sb}<50$ A (plusses) and with $I_{sb}>350$ A (circles). Data with Vlasov antenna.

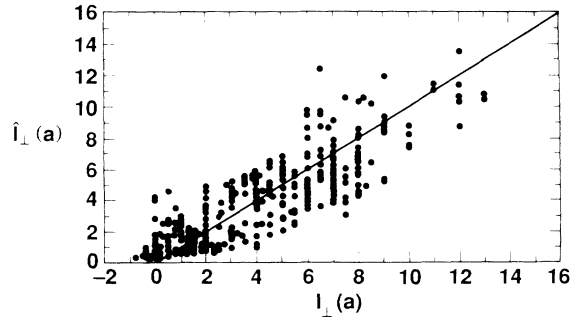

FIG. 3. Predicted $\hat{I}_\perp$ vs measured $I_\perp$ for Vlasov data at $r=19$ cm. Line represents perfect fit.

TABLE I. Summary of Vlasov case. Angular brackets indicate population averages in amperes.

r (cm)	F	$\langle I_\perp \rangle$	$\langle aP^{1/3}Q^{2/3} \rangle$	$\langle bn_{cc}\phi_0 \rangle$	$\langle cI_{si}\phi_0 \rangle$	$\langle dI_{si} \rangle$	$\langle$RT$\rangle$	$\langle$ Eq.(6)$\rangle$
6.5	125	0.87	0.63	0.06	0.05	0.14	0.03	0.8
9.7	87	1.3	0.4	0.51	0.26	0.12	0.16	0.9
13	168	1.9	0.28	0.95	0.55	0.06	0.4	1.1
16	221	2.9	0.34	1.5	0.9	0.07	0.8	1.4
19	200	4.2	1	1.8	1	0.2	1.2	1.7

tions are typically $\pm 30\%$. The ECH term peaks in the core, where it is 75% of $\langle I_\perp \rangle$, consistent with the power deposition profile of the Vlasov antenna. The $n_{cc}\phi_0$ term increases with radius as expected from RT. From the third term, it is found that the sloshing-ion transport is mostly radial at high potential $\phi_0 \simeq 2$ keV. The fourth term contributes most in the core where the beams are focused.

To compare with RT theory, I calculate the ion mobility[4] current

$$I_{\perp m} = 2\pi r L D_\perp e^2 n 2r\phi_0 / r_f^2 T_i, \tag{2}$$

ignoring the $\partial n/\partial r$ and $\partial T_i/\partial r$ terms because $e\phi_0 \gg T_i$ experimentally. The plasma length L is 5 m for the TMX-U central cell. I have taken $\phi = \phi_0(1 - r^2/r_f^2)$ as an approximation to measurements with a heavy-ion beam probe.[12] Since TMX-U is in the plateau regime for $\phi_0 > 200$ V, the diffusion coefficient[3] is $D_\perp \sim \delta r^2 v_i / 4L$ [$v_i = (2T_i/m_i)^{1/2}$ and m_i is the ion mass] with the step size δr determined by geodesic curvature, $\delta r = a_b \sim \rho_i r / L_{tr}$, where ρ_i is the ion Larmor radius. The geodesic curvature scale length $L_{tr} \simeq 25$ cm is determined by following particle orbits.[13] I evaluate $I_{\perp m}$ using the Gaussian density profile ($r_p = 20$ cm) and report the population average $\langle$RT$\rangle$ in Table I. These calculations are 3–30 times smaller than $\langle I_\perp \rangle$, yet they agree with $\langle bn_{cc}\phi_0 \rangle$ within a factor of 2. This shows that RT is not the only transport mechanism in TMX-U.

We can infer an equivalent experimental diffusion coefficient associated with RT by equating $I_{\perp m}$ to the central-cell term $bn_{cc}\phi_0$. This yields

$$D_{\perp \exp} = b r_f^2 T_i \exp(r^2/r_p^2)/4\pi r^2 L e^2$$

with the Gaussian density and parabolic potential profiles. In Fig. 4, $D_{\perp \exp}$ is plotted versus r for $T_i = 60$ eV, which is representative of the data set near $\phi_0 = 1$ kV. The error bars show the standard deviation in b. $D_{\perp \exp}$ increases with radius consistent with theory (solid line), i.e., $a_b^2 \nu_i / 4L$ in the plateau regime, although the measured values are still larger than the theoretical estimates near the axis.

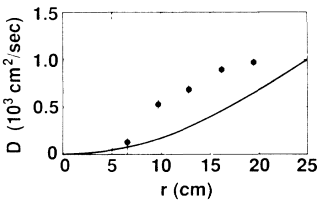

FIG. 4. Diffusion coefficient vs radius for $T_i = 60$ eV ($\phi_0 \simeq 1$ kV). Points inferred from $bn_{cc}\phi_0$ term, solid line is RT calculation in plateau regime.

Using the regression coefficients, I calculate $\hat{I}_\perp$ with the measured independent variables n_{cc}, ϕ_0, etc. for a single shot as shown by the dotted lines in Figs. 1(d) and 1(e). Good agreement is obtained at $r = 6.5$ cm except for $25 < t < 45$ ms. At $r = 19$ cm, excellent agreement is obtained throughout the shot with $\hat{I}_\perp$ reproducing many detailed features. The dashed lines in Figs. 1(d) and 1(e) show the predictions of RT theory $I_{\perp m}$. It is barely detectable in the core and less than 0.2 $I_\perp$ at $r = 19$ cm. In addition, the oscillations of $I_{\perp m}$ and $I_\perp$ are out of phase during the interval $30 < t < 50$ ms indicating clearly that $I_\perp$ is not driven solely by RT.

To gain some understanding of the anomalous transport and to motivate the form of Eq. (1), consider a plasma column which rotates with frequency $\omega_r = 2\phi_0/r_f^2 B$ and is heated asymmetrically with a power density [power/(cross-sectional area)] $p(r)[1 + \epsilon(r)\sin 2\theta]$. I multiply the azimuthal angle θ by 2 to match the quadrupole symmetry of goedesic curvature.[3] As in barbecuing with a rotisserie, the plasma rotation moderates the heating asymmetry when the energy-loss rate ν_e is small ($\nu_d \ll \omega_r$). Therefore, let us postulate that the potential asymmetry in the plasma is

$$\delta\phi/\phi \sim (\nu_e/\omega_r)\epsilon \sin(2\theta)\cos(\pi z/L), \tag{3}$$

where $\nu_e = \nu_\parallel + \nu_\perp$ and $\nu_\parallel$ is the axial loss rate. The ion radial excursion δr averaged over an axial bounce now has an additional component due to the $\mathbf{E}_\theta \times \mathbf{B}$ drift ($E_\theta = 2\delta\phi/r$), namely,

$$\delta r \sim \delta\phi L / r B \nu_i + a_b. \tag{4}$$

Notice that the $\mathbf{E}_\theta \times \mathbf{B}$ drift exceeds the geodesic curvature drift even for small asymmetries, i.e., $e\delta\phi/T_i > 2r^2/LL_{tr}$. To include p explicitly as in Eq. (1), I use the power balance

$$p \sim \nu_e n e \phi L, \tag{5}$$

assuming $e\phi \gg T_i$. Equations (2)–(5) can be solved for

$I_{\perp m}$ in the flow regime[14] where $\nu_{\parallel}=v_i/\sqrt{\pi}RL$ with a mirror ratio $R=7$ for TMX-U. For $\nu_{\parallel}>\nu_{\perp}$, $\delta\phi L/rBv_i>r_l$, I obtain

$$I_{\perp m}\approx\alpha\epsilon^2 p^{1/3}n^{2/3}+\beta r^4 n\sqrt{T_i}\phi_0, \quad (6)$$

where $\alpha=0.4er_f^2/(m_iR^5\delta^2)^{1/3}$ and $\beta=9\sqrt{m_i}/(L_{tr}Br_l)^2$. Since T_i often increases with $e\phi$ in TMX-U, I have defined $\delta\equiv T_i/e\phi$, which is 0.06 ± 0.02 in this data set. Also, the two displacements in Eq. (4) are assumed to be uncorrelated. The first term on the right-hand side of Eq. (6) represents the sole influence of asymmetric heating due to the $\mathbf{E}_\theta\times\mathbf{B}$ drift and motivates the form of the first term in Eq. (1). p is expected to be given primarily by P_Ω because it is the power most strongly coupled to the bulk plasma at low density. The second term in Eq. (6) is the usual RT calculation[3,4] and resembles the second term in Eq. (1). The magnitude of the first term can be estimated by the assumption of constant values of $p=P_\Omega/\pi r_f^2$, and $\epsilon=0.13$. (Such a value of ϵ is on the low side of the 10%–30% azimuthal variation in the plasma-potential control plate potentials[15] when they are floated.) The last column in Table I is the population average of Eq. (6) and compares well with the sum of the first two terms in Eq. (1). Even so, a more self-consistent calculation[16] including the effect of asymmetric heating is preferred.

This analysis was repeated for two other experimental configurations. First, a change of the fundamental ECH antenna[17] produced significant differences in the associated transport. Second, reduction of the geodesic curvature[8] reduced the central-cell component but $I_\perp$ remained significant over all, once again indicating that there are alternative sources of radial transport in TMX-U.

In conclusion, I have found two sources of nonambipolar radial transport in TMX-U in addition to RT; namely, ECH and neutral-beam heating in the end cells. A simple model suggests that the ECH-induced transport is due to asymmetric heating. The transport extends into the central cell, perhaps via the induced azimuthal electric fields, and would apply to other confinement devices[2,6] employing similar heating geometries. The radial sloshing-ion transport occurs in the end cells and may be responsible for their anomalously short lifetime.

The author is indebted to the TMX-U experimental, computer, and technical staffs for their contributions, in particular to C. C. Damm and G. Porter for first noticing the importance of the sloshing beams. It is a pleasure to thank K. K. Anderson, D. E. Baldwin, R. H. Cohen, D. L. Correll, C. C. Damm, G. Francis, J. Myra, P. Poulsen, and T. C. Simonen for useful discussions. This work was supported by the U.S. Department of Energy under Lawrence Livermore National Laboratory contract No. W-7405-ENG-48 and TRW subcontract No. 6625905.

[1]D. P. Grubb *et al.*, Phys. Rev. Lett. **53**, 783 (1984).
[2]M. Inutake *et al.*, Phys. Rev. Lett. **55**, 939 (1985).
[3]D. D. Ryutov and G. V. Stupakov, Dokl. Akad. Nauk SSSR **240**, 1086 (1978) [Sov. Phys. Dokl. **23**, 412 (1978)].
[4]R. H. Cohen, Nucl. Fusion **19**, 1579 (1979).
[5]E. B. Hooper *et al.*, Phys. Fluids **28**, 3609 (1985).
[6]H. R. Garner *et al.*, Nucl. Fusion **26**, 611 (1986).
[7]T. C. Simonen *et al.*, Phys. Rev. Lett. **50**, 1668 (1983).
[8]G. L. Francis *et al.*, Bull. Am. Phys. Soc. **30**, 1377 (1985).
[9]S. N. Vlasov and I. M. Orlova, Izv. Vys. Uchebn. Zav. Radiofiz, **17**, 148 (1974).
[10]J. H. Foote *et al.*, Rev. Sci. Instrum. **57**, 1786 (1986).
[11]J. Johnston, *Econometric Methods* (McGraw-Hill, New York, 1960); N. Draper and H. Smith, *Applied Regression Analysis* (Wiley, New York, 1980), 2nd Ed.
[12]T. C. Simonen *et al.*, in *Proceedings of the Eleventh International Conference on Plasma Physics and Controlled Nuclear Fusion Research, Kyoto, 1986* (International Atomic Energy Agency, Vienna, 1987), Vol. 2, p. 231.
[13]J. H. Foote *et al.*, J. Fusion Energy **2**, 383 (1982).
[14]T. D. Rognlien and T. A. Cutler, Nucl. Fusion **20**, 1003 (1980).
[15]P. Poulsen and B. W. Stallard, private communication.
[16]J. R. Myra *et al.*, Nucl. Fusion **26**, 1655 (1986).
[17]B. Stallard *et al.*, Bull. Am. Phys. Soc. **30**, 1433 (1985).